The Selective Oxidation of Hydrocarbons on Isolated Iron Active Sites under Ambient Conditions

Zhengliang Qi, Junmei Liu, Wanwan Guo and Jun Huang*
State Key Laboratory of Materials-Oriented Chemical Engineering，College of Chemical Engineering，Nanjing Tech University, Nanjing 210009, JiangSu, China.
junhuang@njtech.edu.cn*

(Received on 13th June 2018, accepted in revised form 7th March 2019)

Summary: The N-doped carbon material supported Fe catalysts were developed for the oxidation of C-H bond of hydrocarbons to ketones and alcohols. The supported Fe catalysts were prepared by pyrolysis of $[CMIM]_3Fe(CN)_6$ ionic liquid in activated carbon. And the Fe(Ⅲ)@CN-600 showed good activity and high selectivity for the oxidation of alfa C-H bond of alkylbenzenes. The isolated Fe(Ⅲ) iron active sites should be responsible for the high activity and selectivity for the oxidation of hydrocarbons to ketones. Several ketones were obtained in good to excellent yields. Moreover, cyclohexanone can also be obtained through the oxidation of cyclohexane.

Keywords: Iron, Hydrocarbons, Selective oxidation, Ketones, C-H bond activation.

Introduction

Selective oxidation of saturated hydrocarbons to the corresponding alcohols and ketones is of great essence for the production of fine chemicals in industrial chemistry [1]. Traditionally, noble metal catalysts, including palladium [2], platinum [3], ruthenium [4], and gold [5] are widely investigated and applied for the oxidation of the hydrocarbons due to their high catalytic efficiency. However, the rarity and high cost of noble metals limit the practical application of these catalysts in industry. And recently, catalysts based on Fe, Co were reported for the oxidation of hydrocarbons with good efficiency [6, 7]. Oxygen gas (air) and hydrogen peroxide are preferential green oxidants for oxidation reactions since no other by-products generated from the oxidants except water. Apart from molecular oxygen and hydrogen peroxide, *tert*-buOOH (TBHP) is more active and offers interesting possibilities for oxidation catalysis [8, 9]. For example, TBHP showed improved performance when using several transition-metal catalysts for the epoxidation of olefins [10, 11].

Nitrogen doped carbon materials (NCs) are widely used for various applications based on the versatile properties recently [12-18]. Additionally, we have reported the NCs supported Ir and Rh catalysts for hydrogenation reactions, and good activity and selectivity were obtained [19 a, b]. And the one-step preparation of the Ir and Rh catalysts with NCs supports were developed and the method was used for the preparation of NCs supported Co catalysts, which were applied for the hydrogenation and oxidation reactions with good efficiency [19 c, d]. Besides, we are also interested in the oxidation of hydrocarbons to corresponding alcohols and ketones although it is difficult to activate C-H bonds. Herein, we report a facile preparation of NCs supported Fe catalysts, which encapsulated Fe(Ⅲ) species into the nitrogen-doped carbon materials via the pyrolysis of IL 1-cyanomethyl -3-methylimidazolium ferricyanide $[CMIM]_3Fe(CN)_6$ in activated carbon (Scheme-1). The Fe catalysts were highly active and selective for the oxidation of hydrocarbons with TBHP as oxidant at ambient conditions.

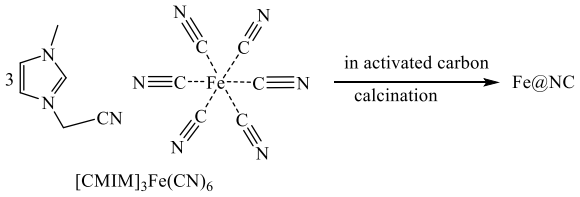

Scheme-1: The preparation of Fe(III)@NC catalysts by pyrolysis of $[CMIM]_3Fe(CN)_6$ in activated carbon.

Experimental

Materials and methods

All the reagents and chemicals were purchased from commercial sources (Aladdin

*To whom all correspondence should be addressed.

Reagent Company) and used without any further purification. ^{1}H-NMR spectra were measured with a Bruker ASCEND 400 spectrometer (Germany) in $CDCl_3$ using tetramethylsilane (TMS) as internal reference. X-ray photoelectron spectroscopy (XPS) data were obtained with an ESCAL ab220i-XL electron spectrometer from VG Scientific using 300 W AlKa radiations (England). X-ray diffraction (XRD) patterns were collected on the Bruker D8 Advance powder diffractometer (Germany) using Ni-filtered Cu Kα radiation source at 40 Kv and 20 mA, from 5º to 80º with a scan rate of 0.5º /min. The base pressure was about $3x10^{-9}$ mbar. Scanning Electron Microscope (SEM) images were performed on a HITACHI S-4800 field-emission scanning electron microscope (Japan), HAADF-STEM and Transmission Electron Microscope (TEM) images were obtained using a JEOL JEM-2010 (200 kV) TEM instrument (Japan). BET surface areas were measured at the temperature of liquid nitrogen using a Micromeritics ASAP2010 analyzer (America). The samples were degassed at 150 ºC under vacuum of 10^{-3} Torr before analysis. ^{57}Fe Mössbauer spectra of the catalyst were carried out on a German Wissel-MS500 at room temperature. The radioactive source was ^{57}Co (Pd) moving in a constant acceleration mode. Raman spectra of the samples were carried out using a RENISHAW-2000 Raman Spectrometer (England). Thermogravimetry analysis (TGA) was carried out with a STA409 instrument (Germany) under dry air at a heating rate of 10 ºC/min. Elemental analyses were performed on a CHN elemental analyzer (FlashEA 1112, America).

Catalyst preparation

The ionic liquid [CMIM]Cl was synthesized as following. A mixture of 1-methylimidazole (Aladdin, 99 wt.%, 8.29 g, 100 mmol) and $ClCH_2CN$ (Aladdin, 98 wt.%, 9.24 g, 120 mmol) was stirred at room temperature for 24 h, and white solid was formed. The solid was then washed with diethyl ether (3*50 ml) and dried under vacuum for 24 h. The [CMIM]Cl was obtained in 96% yield (15.1 g).

The typical procedure for the preparation of the catalysts is described as following. A mixture of $K_3Fe(CN)_6$ (Aladdin, 99.5 wt.%, 2.0 mmol, 661.8 mg) and [CMIM]Cl (6.0 mmol, 945.6 mg, Fe: [CMIM]Cl = 1:3 mole ratio) in 20 ml water was stirred for 30 minutes at room temperature (When using $K_4Fe(CN)_6$ as Fe source, Fe: [CMIM]Cl = 1:4 mole ratio, $K_4Fe(CN)_6$, Aladdin, 99.5 wt.%). Then, the 1.0 g of activated carbon powder (Nanjing XFNano Tech) was added and the whole reaction mixture was stirred at 60 ºC overnight. The reaction mixture was cooled to room temperature and water was removed slowly under vacuum. The remaining solid sample obtained was dried at 60 ºC for 12 h. Then solid sample was pyrolyzed to Fe(Ⅲ)@CN-600 at 600 ºC for 2 h under nitrogen atmosphere. The Fe(Ⅲ)@IL-600 catalyst was synthesized without adding activated carbon powder with similar conditions. The Fe(Ⅲ)@AC-600 catalyst was synthesized without adding $[CMIM]_3Fe(CN)_6$ with similar conditions.

General procedure for oxidation of C-H bond

The selective oxidation of ethylbenzene was carried out in a 25 ml glass tube within 6.0 ml water as solvent at room temperature within 7-12 h under continuous stirring. Catalyst Fe(Ⅲ)@CN-600, water, oxidant TBHP and ethylbenzene were added into the glass tube, then the reaction tube was sealed with stirring. When the reaction was finished, 2.0 ml ethyl acetate was added to the reaction mixture, and the liquid sample was detected with gas chromatography.

The reusing of Fe(Ⅲ)@CN-600 was as following. The catalyst Fe(Ⅲ)@CN-600 was filtered and washed with ethanol (10 ml*3) after reaction, then dried under vacuum at 60 ºC for 12 h. And then the recycled Fe(Ⅲ)@CN-600 was used for the next reaction cycle.

Results and Discussion

Catalyst characterization

The catalysts were characterized by XRD and the resulted spectra were presented in Fig. 1. Two weak broaden peaks centered at 25º and 43º were observed for the Fe(Ⅲ)@CN-600 corresponding to the (002) and (004) planes of carbon materials (Fig. 1, curve c) [20]. The NC material was formed from pyrolysis of $[CMIM]_3Fe(CN)_6$, but no aggregation of Fe can be found at about 600 ºC. No obvious peaks for Fe metal and Fe oxide phases were found in all these materials (Fig. 1), which is in accordance with Raman results (Fig. S1, SI). When the pyrolysis temperature was up to 800 ºC, some new peaks formed in the region of 40º-50º (Fig. 1, curve d), which were assigned to Fe_3C species at high temperature [21].

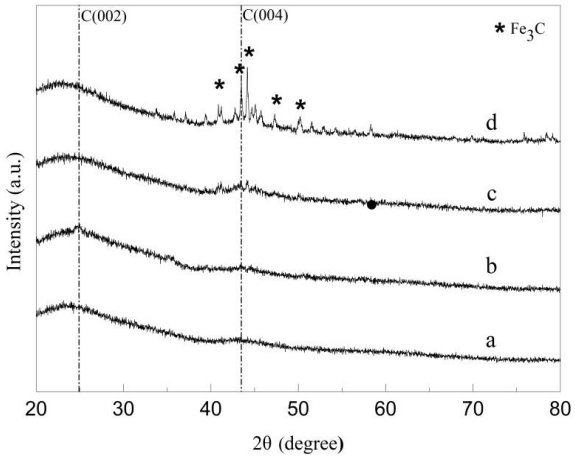

Fig. 1: The XRD spectra of a. Fe(Ⅱ)@CN-600 (pyrolysis of $[CMIM]_4Fe(CN)_6$ in activated carbon), b. Fe(Ⅲ)@CN-400, c. Fe(Ⅲ)@CN-600, d. Fe(Ⅲ)@CN-800.

The SEM images were presented as Fig. 2, irregular morphology surface was found for all 3 samples pyrolysed under 400 ºC, 600 ºC and 800 ºC respectively. The BET specific surface areas of materials Fe(Ⅲ)@CN-400, Fe(Ⅲ)@CN-600 and Fe(Ⅲ)@CN-800 were 304.41 m^2/g, 498.54 m^2/g and 582.81 m^2/g respectively. And the pore volumes of Fe(Ⅲ)@CN-400, Fe(Ⅲ)@CN-600 and Fe(Ⅲ)@CN-800 were 0.17 cm^{-3}/g, 0.27 cm^{-3}/g and 0.31 cm^{-3}/g respectively. The average pore diameters of Fe(Ⅲ)@CN-400, Fe(Ⅲ)@CN-600 and Fe(Ⅲ)@CN-800 were 2.22 nm, 2.15 nm and 2.13 nm respectively. The BET specific surface area, pore diameters and the pore volume were decreased obviously comparing to the parent activated carbon, as the N hybrid carbon was formed from $[CMIM]_3Fe(CN)_6$ in the activated carbon (Table-1 and Fig. 3).

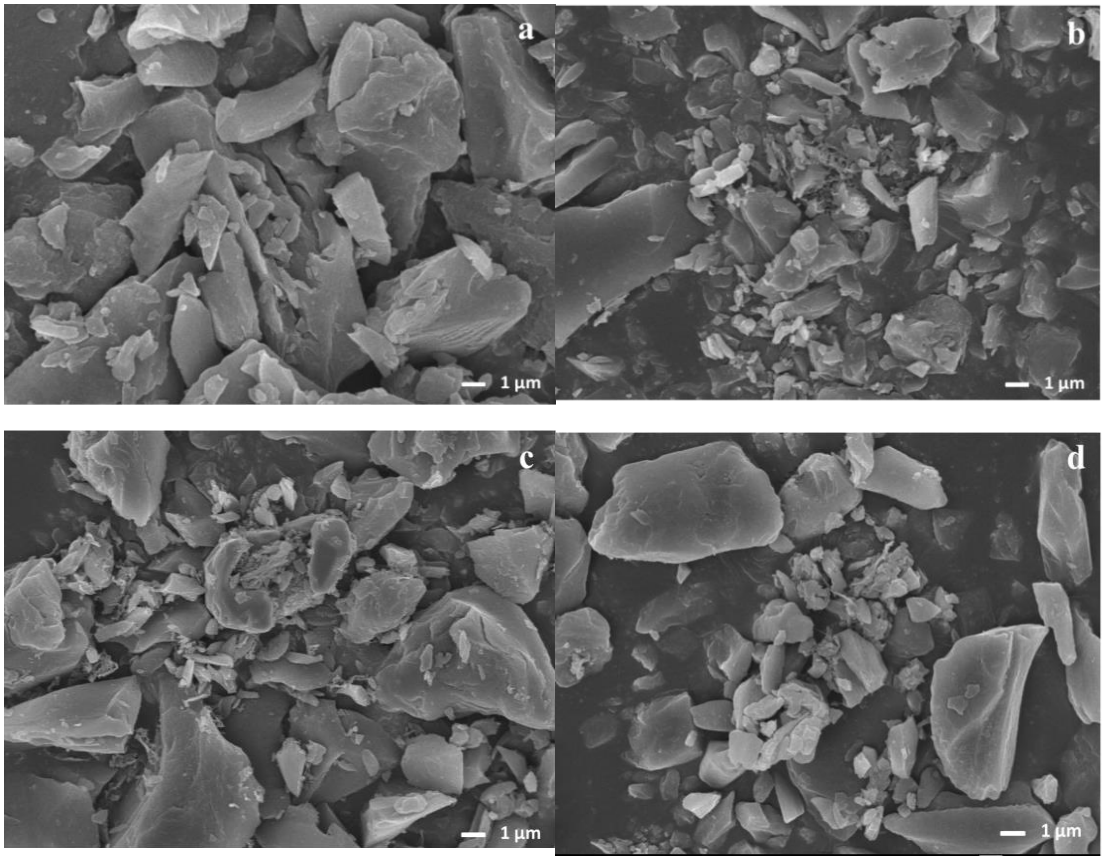

Fig. 2: The SEM images of a. Fe(Ⅲ)@CN-400, b. Fe(Ⅲ)@CN-600, c. Fe(Ⅲ)@CN-800, d. Recycled Fe(Ⅲ)@CN-600.

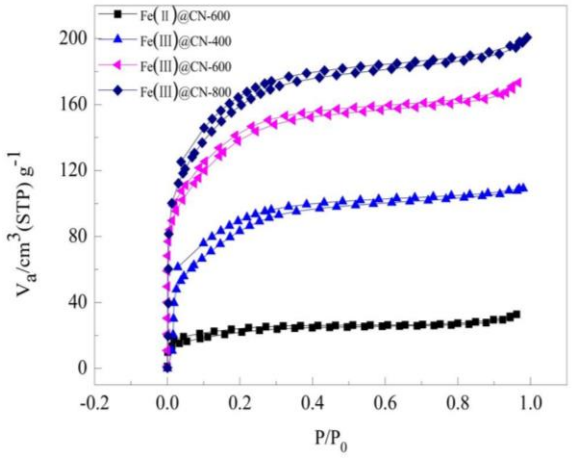

Fig. 3: Nitrogen adsorption-desorption isotherms of a. Fe(Ⅱ)@CN-600, b. Fe(Ⅲ)@CN-400, c. Fe(Ⅲ)@CN-600, d. Fe(Ⅲ)@CN-800.

Table-1: BET data of a. Fe(Ⅱ)@CN-600, b. Fe(Ⅲ)@CN-400, c. Fe(Ⅲ)@CN-600, d. Fe(Ⅲ)@CN-800.

Entry	Catalyst	$a_{s,BET}$ [$m^2\ g^{-1}$]	Mean pore diameter [nm]	Total pore volume [$cm^3\ g^{-1}$]
a	Fe(Ⅱ)@CN-600	77.178	2.6302	0.0507
b	Fe(Ⅲ)@CN-400	304.41	2.2177	0.1688
c	Fe(Ⅲ)@CN-600	498.54	2.1500	0.2680
d	Fe(Ⅲ)@CN-800	582.81	2.1285	0.3101

According to HAADF-STEM images (Fig. 4, a), no Fe metal or FeO_x particles can be seen from catalyst Fe(Ⅲ)@CN-600, which is in agreement with the XRD patterns and Raman results. The elemental mapping of Fe in Fe(Ⅲ)@CN-600 showed that the Fe element is well dispersed in catalyst (Fig. 4, d). No aggregated Fe or FeOx were found even at high resolution TEM (Fig. 4, e), which means that the Fe in Fe(Ⅲ)@CN-600 was mainly as isolated Fe(Ⅲ)-C or Fe(Ⅲ)-N species but not FeO_x particles. Additionally, the N element in Fe(Ⅲ)@CN-600 is along well with the distribution of Fe element (Fig. 4, c, d).

The element analysis was performed and the results are showed in Table-2. With the increase of pyrolysis temperature, the C content in catalysts was increased while N contents decreased, since some small N-containing molecules were formed and emitted by decomposition of NCs at high temperature [12 a]. The N content of Fe(Ⅲ)@CN-400, Fe(Ⅲ)@CN-600 and Fe(Ⅲ)@CN-800 were 9.97 %, 6.33 % and 2.37 % respectively.

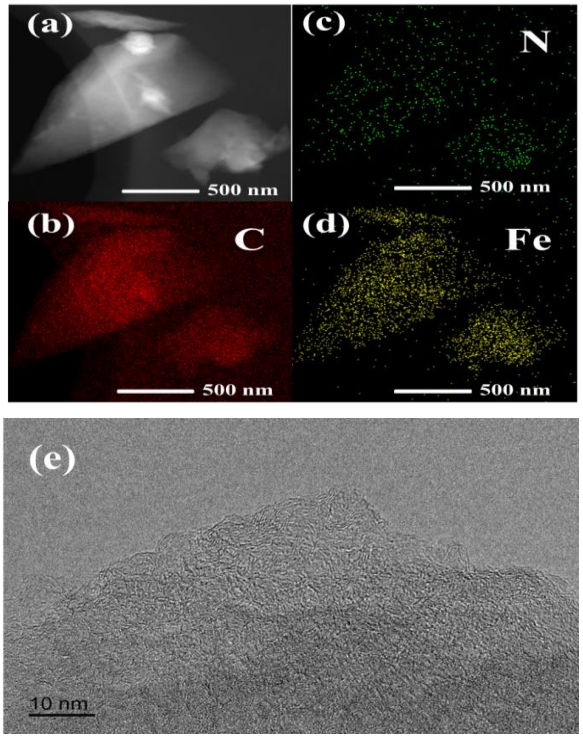

Fig. 4: The HAADF-STEM image (a), element mapping images of C, N, Fe (b, c, d) and the HRTEM image (e) of Fe(Ⅲ)@CN-600 catalyst.

Table-2: The element analysis results of a. Fe(Ⅱ)@CN-600, b. Fe(Ⅲ)@CN-400, c. Fe(Ⅲ)@CN-600, d. Fe(Ⅲ)@CN-800.

Entry	Catalyst	C	N	H
a	Fe(Ⅱ)@CN-600	46.89	8.13	2.019
b	Fe(Ⅲ)@CN-400	53.62	9.97	1.611
c	Fe(Ⅲ)@CN-600	54.25	6.33	1.562
d	Fe(Ⅲ)@CN-800	58.43	2.37	1.689

Besides, XPS was carried out to detect the chemical state of Fe in the Fe(Ⅲ)@CN-600 catalyst (Fig. 5). There are two peaks at binding energies of 711.7 eV (Fe $2p_{3/2}$) and 724.5 eV(Fe $2p_{1/2}$) for Fe^{3+} species respectively (Fig. 5, curve c) [22]. Fe in Fe(Ⅲ)@CN-600 is mainly as Fe^{3+} species [23], and could be reduced to Fe^{2+} or Fe at 800 °C (Fig. 5, curve d for Fe(Ⅲ)@CN-800). The XPS spectra of N 1s in Fe(Ⅲ)@CN-600 can be deconvoluted into three peaks with binding energies at 398.7 eV, 400.4 eV, and 405.3 eV (Fig. 6, curve c), which are assigned to pyridinic N, graphitic N, and N-oxide (N^+-O^-) respectively [24]. Pyridinic N is the dominant phase in the samples of Fe(Ⅲ)@CN-400 and

Fe(Ⅲ)@CN-600, but graphitic N becomes the dominant one in the sample Fe(Ⅲ)@CN-800 as the pyridinic N transformed into graphitic N [25].

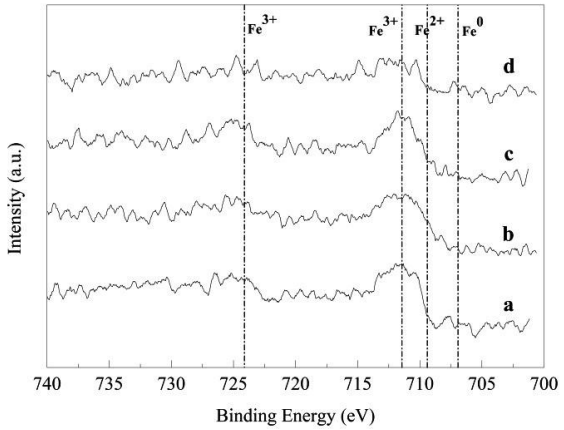

Fig. 5: The XPS spectra of Fe 2p for a. Fe(Ⅱ)@CN-600, b. Fe(Ⅲ)@CN-400, c. Fe(Ⅲ)@CN-600, d. Fe(Ⅲ)@CN-800.

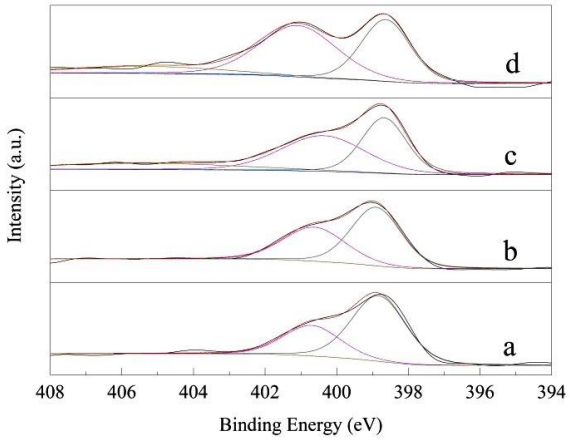

Fig. 6: The XPS N 1s spectra of a. Fe(Ⅱ)@CN-600, b. Fe(Ⅲ)@CN-400, c. Fe(Ⅲ)@CN-600, d. Fe(Ⅲ)@CN-800.

Mössbauer spectroscopy is a mighty means to distinguish different Fe species. The Mössbauer spectra of catalyst Fe(Ⅲ)@CN-600 is showed in Fig. 7 and relative Mössbauer parameters and the assignment of different Fe species were listed in Table-3. The spectra could be well-fitted with three doublets. There is no sextet or singlet could be observed, which testifies the absence of Fe^0 species [26]. Based on the values of isomer shift (IS) and quadrupole splitting (QS) (Table-3), three different doublets can be distinguished. D1, which has relatively larger values of IS and QS, can be assigned to FePc-like $Fe^{II}N_4$ species [27, 28]. The relatively low content explains the absence of Fe^{2+} species in XPS results (Fig. 5). D2, with an IS value of 0.33 and a QS value of 0.63, can be assigned to ferric X-$Fe^{III}N_4$-Y species (X and Y refer to O or N ligand), in which the Fe atom is slightly pulled out of the N_4 plane, resulting in a distorted octahedral structure [29]. In this case, the six-coordinate Fe^{3+} compound is coordination saturated and not accessible by oxygen molecules, thus, it is unable to work as active sites. The D3 was assigned to a penta-coordinated N-$Fe^{III}N_4$ compound, which has an unoccupied site to adsorb oxygen in the axial direction perpendicular to the Fe-N_4 plane. Based on the above analysis, it is reasonable to assume D3 Fe species as the real catalytically active sites for its unsaturated coordination [30].

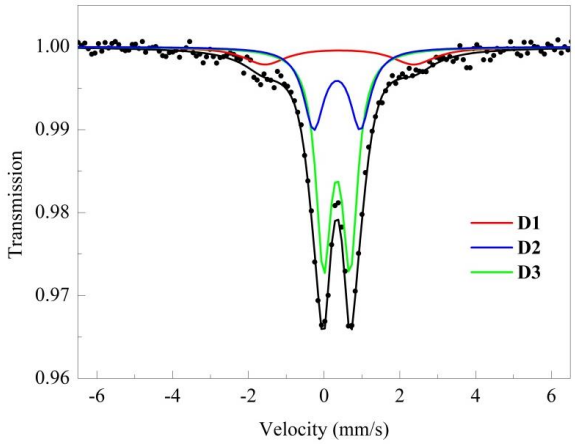

Fig. 7: ^{57}Fe Mössbauer spectra of the Fe(Ⅲ)@CN-600.

Table-3: Summary of the Mössbauer parameters and assignments to different iron species in Fe(Ⅲ)@CN-600.

Fe species	IS(mm/s)	QS(mm/s)	area%	assignment
D1	0.38	4.14	9.1	$Fe^{II}N_4$
D2	0.33	0.63	24.8	X-$Fe^{III}N_4$-Y
D3	0.34	0.85	66.1	N-$Fe^{III}N_4$

TGA of $K_3Fe(CN)_6$ showed that free water was removed below 200 °C, and $K_3Fe(CN)_6$ was stable until 500 °C (Fig 8a). The stability of $K_3Fe(CN)_6$ indicated that the condensation process of $[CMIM]_3Fe(CN)_6$ was started from the cation [CMIM] because anion $Fe(CN)_6$ is quite stable. Along further elevating the pyrolysis temperature, the weight loss increased gradually (Fig. 8a). The TGA of $[CMIM]_3Fe(CN)_6$ in activated carbon suggested the formation of Fe(Ⅲ)@CN-400, Fe(Ⅲ)@CN-600 and Fe(Ⅲ)@CN-800 (Fig. 8b). With the increasing of the

temperature, Fe(Ⅲ)@CN materials were formed through condensation of the $[CMIM]_3Fe(CN)_6$ with slightly decomposition.

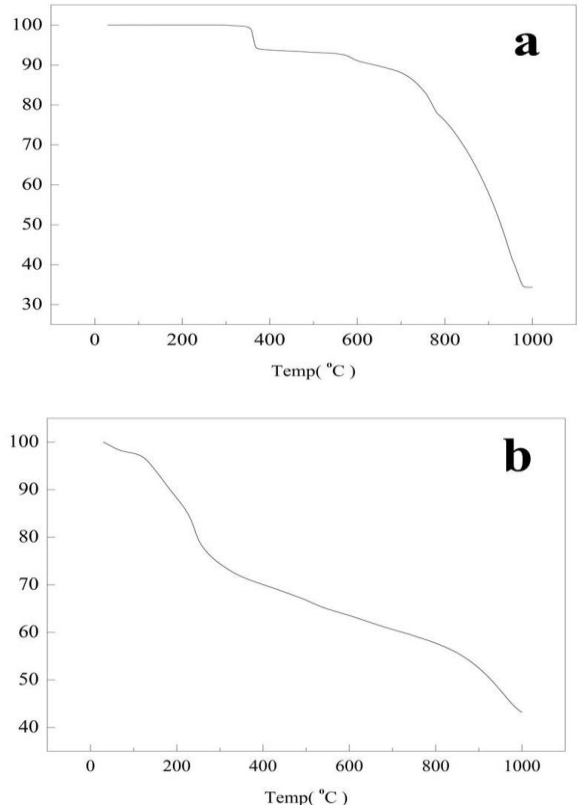

Fig. 8: TGA analysis for a. $K_3Fe(CN)_6$, b. Fe(Ⅲ)@CN-600* (before pyrolysis).

The oxidation of ethylbenzene to acetophenone under different conditions

The oxidation of ethylbenzene was used as model reaction for the optimization of the reaction conditions, and the results are listed in Table-4. In the 4 prepared catalysts, Fe(Ⅲ)@CN-600 was found to be most active for the oxidation of ethylbenzene and acetophenone was obtained in 98% yield with 99% selectivity at room temperature (Table-4, entries 1-4, 5). Catalyst without activated carbon Fe(Ⅲ)@IL-600 was not active enough, and the conversion of ethylbenzene was only 23%. Catalyst Fe(Ⅲ)@AC-600 ($K_3Fe(CN)_6$ in activated carbon) was not active at all, and acetophenone was obtained in 4% yield (Table-4, entries 6, 7). Besides, H_2O_2 and oxygen gas are not efficient oxidants, and only negligible acetophenone was obtained. Increasing of the oxygen pressure from 1.0 atm to 1.0 MPa cannot improve the reaction conversion (Table-4, entries 8-10). $K_3Fe(CN)_6$ and $K_4Fe(CN)_6$ are not active catalyst, and only small amount of acetopheone was detected (Table-4, entries 12, 13). Only trace acetophenone was found when no TBHP or Fe(Ⅲ)@CN-600 added in the reaction system (Table-4, entries 11, 14).

Table-4: The optimization of reaction conditions for the oxidation of ethylbenzene to acetopheone.

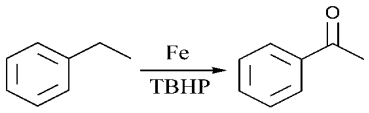

Entry [a]	Catalyst	Con(%)	Sel(%)
1	Fe(Ⅱ)@CN-600	64	99
2	Fe(Ⅲ)@CN-400	43	99
3	Fe(Ⅲ)@CN-600	83	99
4[b]	Fe(Ⅲ)@CN-600	98	99
5	Fe(Ⅲ)@CN-800	70	99
6	Fe(Ⅲ)@ILs-600	23	99
7	Fe(Ⅲ)@AC-600	4	83
8[c]	Fe(Ⅲ)@CN-600	1	99
9[d]	Fe(Ⅲ)@CN-600	1	99
10[e]	Fe(Ⅲ)@CN-600	5	99
11[f]	Fe(Ⅲ)@CN-600	2	99
12[g]	$K_3Fe(CN)_6$	20	95
13[h]	$K_4Fe(CN)_6$	9	93
14[i]	none	1	-

[a] Reaction conditions: 4.0 mol % Fe catalyst; 0.5 mmol of ethylbenzene (61 µl); 3.5 mmol of TBHP (500 µl); 2.0 ml of H_2O; for 7 h; at rt; The conversion and selectivity were determined by GC analysis with dodecane as an internal standard. [b] Fe catalyst, 8.0 mol % added; with 6.0 ml of H_2O; for 12 h. [c] H_2O_2 (354 µl) 3.5 mmol used as oxidant. [d] O_2 under 1.0 atm as oxidant. [e] O_2 under 1.0 MPa as oxidant. [f] Without TBHP. [g] $K_3Fe(CN)_6$ 0.02 mmol added. [h] $K_4Fe(CN)_6$ 0.02 mmol added. [i] Without Fe catalyst.

The applying scope of Fe(Ⅲ)@CN-600 for the oxidation reaction

With Fe(Ⅲ)@CN-600 as catalyst, the applying scope of the oxidation reaction was investigated, and the results are presented in Table-5. As shown in Table-5, ethylbenzene with Br, NO_2 groups were transformed smoothly into corresponding ketones in high yields respectively (Table-5, entries 2, 3). Moreover, *n*-propylbenzene and *n*-butylbenzene were oxidized to the corresponding ketones in 78% and 92% yields respectively (Table-5, entry 4, 5). The Fe(Ⅲ)@CN-600 catalyzed oxidation of *i*-butylbenzene gave 2-methyl-1-phenylpropan-1-one in 50% yield with good selectivity, which showed the steric hindrance of the branch methyl group (Table-5, entry 6). Cumene can be oxidized to cumyl alcohol in good yield (Table-5, entry 7). In addition, the oxidation of diphenylmethane, 2-benzylpyridine and xanthene afforded the related benzophenone, 2-benzoylpyridine and xanthen-9-one in 99%, 93% and 95% yields respectively (Table-5, entries 8-10). Tetralin and indane can be transformed into 3,4-dihydronaphthalen-1(2H)-one and 2,3-dihydro-1H-inden-1-one in 69% and 52% yields

respectively (Table-5, entries 11-12). Besides, cyclohexanone could be obtained through the oxidation of cyclohexane (Table-5, entry 13).

Table- 5: The selective oxidation of hydrocarbons with Fe(Ⅲ)@CN-600 catalyst.

Entry [a)]	substrate	product	Time/h	Con%	Yield [b]%
1 [ref 1]	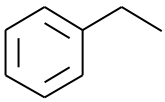	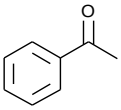	12	98	97
2 [ref 1]	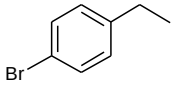	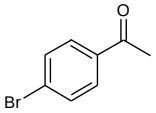	12 18	92 97	92 97
3 [ref 1]	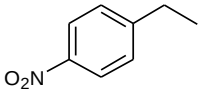	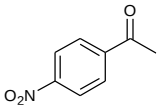	12 18	86 91	86 91
4 [ref 1]	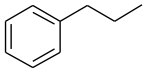	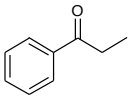	12 18	70 78	70 78
5 [ref 1]	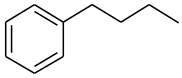	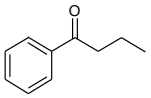	48	92	92
6 [ref 2]	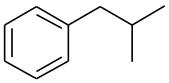	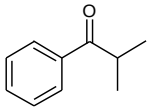	48	50	50
7 [ref 3]	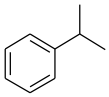	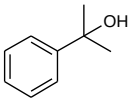	12 18	96 97	90 91
8 [ref 4]	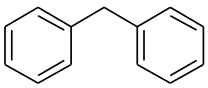	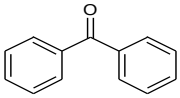	12	99	99
9 [ref 4]	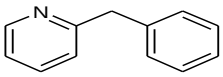	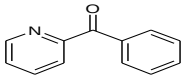	12 18	81 93	81 93
10 [ref 5]	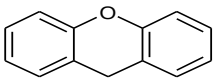	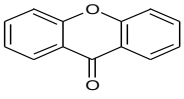	24	95	95
11 [ref 4]	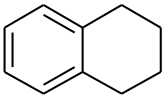	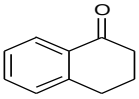	24	76	69
12 [ref 4]	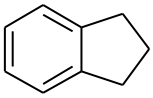	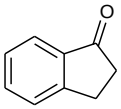	12 18	51 52	51 52

13 [ref 2]	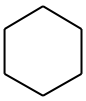	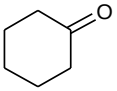	18	61	61

a) Reaction conditions: 8.0 mol % Fe catalyst (34.0 mg); 0.5 mmol of substrate; 3.5 mmol of TBHP (500 µl), 6.0 ml H_2O, at room temperature. [b] Isolated yield.

The performance of the Fe(Ⅲ)@CN-x catalysts is based on the local environment of the Fe center. The $K_3Fe(CN)_6$ is less active for the selective oxidation of C-H bond (Table-4, entry 12) because it is FeC_6 species. During the pyrolysis process, the condensation occurred and the Fe(Ⅲ)@CN-x catalysts were formed after 400 °C (Fig. 8, curve b). The Fe center in catalyst Fe(Ⅲ)@CN-400 was similar as in $K_3Fe(CN)_6$, since the condensation did not start at 400 °C. Catalyst Fe(Ⅲ)@CN-600 is more active than Fe(Ⅲ)@CN-400 because the condensation of the $[CMIM]_3Fe(CN)_6$ improved the activity, and we assume the condensation process changed FeC_6 species to FeC_nN_{5-n} species along with the formation of the N hybrid graphene. It is reported that the 5 coordinated species FeN_5 was the most active species for the selective oxidation of C-H bond [31, 32]. But in Fe(Ⅲ)@CN-800, the N content reduced to 2.4% and Fe_3C formed [21] (Table-2), so the activity was not as high as Fe(Ⅲ)@CN-600. The isolated iron active sites are more active than the Fe_3C sites for the selective oxidation of C-H bond.

The reusability of Fe(Ⅲ)@CN-600 for the oxidation of ethylbenzene

The reusability of the Fe(Ⅲ)@CN-600 was tested for the oxidation of ethylbenzene and the results are shown in Fig. 9. The Fe(Ⅲ)@CN-600 can be reused at least 5 times without obvious loss of activity. The slightly deactivation may be due to the mass loss of the catalyst in the recycle processes (filtration and collection the catalyst). Moreover, no Fe was detected (ICP-AES) in the solution after removal of the catalyst by filtration. The BET surface areas decreased sharply after the reaction (498 vs 295 m^2/g) due to the loss of tiny carbon powder during the recovering process (Fig. 2, b and d), Nitrogen adsorption-desorption isotherms of Fe(Ⅲ)@CN-600 after five cycles of reaction remained as typical Type Ⅰ curve. Moreover, XRD, TEM , and SEM (Fig. 2 d) characterizations show that the splendid dispersion of Fe species is well-preserved after the five repetitive runs. The XPS spectra of Fe 2p of reused Fe(Ⅲ)@CN-600 has a weaker peek at 724.5 eV(Fe $2p_{1/2}$) than that of fresh catalyst, however, Fe species are still remain as Fe^{3+}. These evidences explicitly demonstrate the excellent stability and recycling ability of catalyst Fe(Ⅲ)@CN-600.

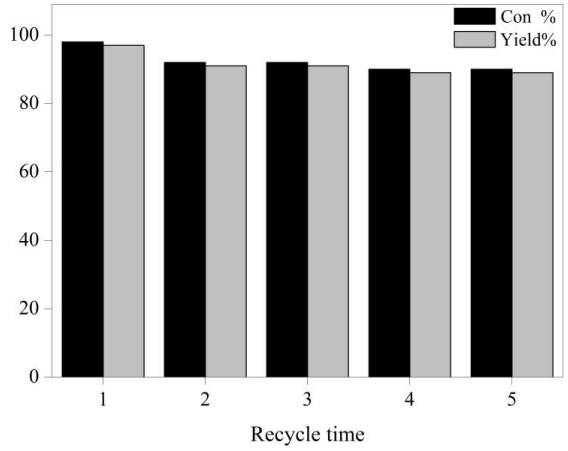

Fig. 9: The reusability of Fe(Ⅲ)@CN-600 for the oxidation of ethylbenzene.

Conclusion

In conclusion, we demonstrated the N-doped carbon supported Fe catalysts for the oxidation of C-H bond to ketones and alcohol. The N-doped carbon supported Fe catalysts were prepared by pyrolysis of $[CMIM]_3Fe(CN)_6$ ionic liquid in activated carbon. And the Fe(Ⅲ)@CN-600 showed good activity and high selectivity for the oxidation of alfa C-H bond of alkylbenzenes. The isolated Fe(Ⅲ) species should be responsible for the high activity and selectivity for the oxidation of hydrocarbons to ketones. Several ketones were obtained in good to excellent yields. Moreover, cyclohexanone can also be obtained through the oxidation of cyclohexane.

Acknowledgements

This work was supported by the National Natural Science of Foundation of China (grant No. 21676140), and the fund from the State Key Laboratory of Materials-Oriented Chemical Engineering (grant ZK201711).

References

1. D. H. Barton and D. Doller, The Selective

Functionalization of Saturated Hydrocarbons: Gif Chemistry, *Acc. Chem. Res*., **25,** 504 (1992).

2. B. Q. Zhang, H. L. Peng, L. J. Yang, H. L. Li, H. X. Nan, Z. X. Liang, H. Y. Song, H. N. Su, C. Li and S. J. Liao, Three dimensional palladium nanoflowers with enhanced electrocatalytic activity towards the anodic oxidation of formic acid, *J. Mater. Chem. A*, **3,** 973 (2015).
3. T. Zimmermann, M. Soorholtz, M. Bilke, F. Schuth, Selective methane oxidation catalysed by platinum salts in oleum at turnover frequencies of large-scale industrial processes, *J. Am. Chem. Soc*., **138,** 12395 (2016).
4. Y. C. Zhang, L. Y. Zhao, H. G. Zhang, R. Huang, J. Q. Zhao, Oxidation of alkanes and secondary alcohols to ketones with tertbutyl hydroperoxide catalyzed by a water-soluble ruthenium complex under solvent-free conditions, *Appl. Organometal. Chem*., **31,** 3709 (2017).
5. L. P. Qian, Z. Wang, E. V. Beletskiy, J. Y. Liu, H. J. Santos, T. H. Li, M. C. Rangel, M. C. Kung & H. H. Kung, Stable and solubilized active Au atom clusters for selective epoxidation of cis-cyclooctene with molecular oxygen, *Nat. Commun*., **8,** 14881 (2017).
6. S. Yamaguchi, Y. Miyake, K. Takiguchi, D. Ihara, H. Yahiro, Oxidation of cyclic hydrocarbons with hydrogen peroxide over iron complexes encapsulated in cation-exchanged zeolite, *Catal. Today*, **303,** 249 (2018).
7. P. Shringarpure, A.Patel, Cobalt(II) exchanged supported 12-tungstophosphoric acid: synthesis, characterization and non-solvent liquid phase aerobic oxidation of alkenes, *J. Mol. Catal. A: Chem*., **321,** 22 (2010).
8. X. F. Wu, J. L. Gong and X. X. Qi, A powerful combination: recent achievements on using TBAI and TBHP as oxidation system, *Org. Biomol. Chem.*, **12,** 5807 (2014).
9. M. B. Zhou, R. J. Song, X. H. Ouyang, Y. Liu, W. T. Wei, G. B. Deng and J. H. Li, Metal-free oxidative tandem coupling of activated alkenes with carbonyl C(sp^2)-H bonds and aryl C(sp^2)-H bonds using TBHP, *Chem. Sci*., **4,** 2690 (2013).
10. M. Islam, P. Mondal, S. Mukherjee, M. Mobarak, A. S. Roy, S. Mondal and S. Sarkar, Efficient liquid phase oxidation of olefins and aromatic alcohol catalyzed by reusable polymer anchored Schiff base complexes, *J. Chem. Technol. Biotechnol*., **85,** 460 (2010).
11. C. Anand, P. Srinivasu, G. P. Mane, S. N. Talapaneni, M. R. Benzigar, S. V. Priya, S. S. Al-deyab, Y. Sugi, A. Vinu, Direct synthesis and characterization of highly ordered cobalt substituted KIT-5 with 3D nanocages for cyclohexene epoxidation, *Micropor. Mesopor. Mat*., **167,** 146 (2013).
12. a) J. S. Lee, X. Wang, H. Luo, G. A. Baker, S. Dai, Facile ionothermal synthesis of microporous and mesoporous carbons from task specific ionic liquids, *J. Am. Chem. Soc*., **131,** 4596 (2009); b) Z. Y. Zhang, G. M. Veith, G. M. Brown, P. F. Fulvio, P. C. Hillesheim, S. Dai and S. H. Overbury, Ionic liquid derived carbons as highly efficient oxygen reduction catalysts: first elucidation of pore size distribution dependent kinetics, *Chem. Commun*., **50,** 1469 (2014); c) G. J. Liu, K. Huang, Q. Wu, S. Dai, Solvent-free self-assembly to the synthesis of nitrogen-doped ordered mesoporous polymers for highly selective capture and conversion of CO_2, *Adv. Mater*., **29,** 1700445 (2017); d) X. Zhu, C. C. Tian, S. H. Chai, K. Nelson, K. S. Han, E. W. Hagaman, G. M. Veith, S. M. Mahurin, H. L. Liu and S. Dai, New tricks for old molecules: development and application of porous N-doped, carbonaceous membranes for CO_2 separation, *Adv. Mater*., **25,** 4152 (2013).
13. T. Song, P. Ren, Y. Duan, Z. Wang, X. Chen and Y. Yang, Cobalt Nanocomposites on N-Doped Hierarchical Porous Carbon for Highly Selective Formation of Anilines and Imines from Nitroarenes, *Green Chem.*, **20**, 4629 (2018).
14. D. Nandan, G. Zoppellaro, I. Medrik, C. Aparicio, P. Kumar, M. Petr, O. Tomanec, M. B. Gawande, R. S. Varma and R. Zboril, Cobalt-entrenched N-, O-, and S-tridoped carbons as efficient multifunctional sustainable catalysts for base-free selective oxidative esterification of alcohols, *Green Chem*., **20**, 3542 (2018).
15. J. J. Huo, P. Duan, H. N. Pham, Y. J. Chan, A. K. Datye, K Schmidt-Rohr and B. H. Shanks, Improved hydrothermal stability of Pd nanoparticles on nitrogen-doped carbon supports, *Catal. Sci. Technol*., **8**, 3548 (2018).
16. L. Roldan, Y. Marco, and Enrique Garcia-Bordeje, Origin of the Excellent Performance of Ru on Nitrogen-Doped Carbon Nanofibers for CO_2 Hydrogenation to CH_4, *ChemSusChem*., **9**, 1 (2016).
17. Y. S. Ren, Z. L. Yuan, K. Lv, J. Sun, Z. H. Zhang and Q. Chi, Selective and metal-free oxidation of biomass derived 5-hydroxymethylfurfural to 2,5-diformylfuran over nitrogen-doped carbon materials, *Green Chem*., **20**, 4946 (2018).
18. J. K. Wang, Q. H. Deng, Y. J. Wang, Tunable

oxidation state of Co in CoOx@N-doped graphene derived from PANI/Co_3O_4 and the enhanced oxygen reduction catalysis, *Appl. Surf. Sci.*, **465**, 665 (2019).

19. a) L. Huang, Z. Wang, L. F. Geng, R. Z. Chen, W. H. Xing, Y. Wang, J. Huang, Selective and recyclable rhodium nanocatalysts for the reductive N-alkylation of nitrobenzenes and amines with aldehydes, *RSC. Adv*., **5,** 56936 (2015); b) Z. Wang, L. Huang, L. F. Geng, R. Z. Chen, W. H. Xing, Y. Wang, J. Huang, Chemoselective transfer hydrogenation of aldehydes and ketones with a heterogeneous iridium catalyst in water, *Catal. Lett.*, **145,** 1008 (2015); c) F. Mao, D. J. Sui, Z. L. Qi, H. P. Fan, R. Z. Chen, J. Huang, Heterogeneous cobalt catalysts for reductive amination with H_2: general synthesis of secondary and tertiary amines, *RSC. Adv*., **6,** 94068 (2016); d) F. Mao, Z. L. Qi, H. P. Fan, D. J. Sui, R. Z. Chen, J. Huang, Heterogeneous cobalt catalysts for selective oxygenation of alcohols to aldehydes, esters and nitriles, *RSC. Adv*., **7,** 1498 (2016).
20. L. L. Fan, P. F. Liu, X. C. Yan, L. Gu, Z. Z. Yang, H. G. Yang, S. L. Qiu, X. D. Yao, Atomically isolated nickel species anchored on graphitized carbon for efficient hydrogen evolution electrocatalysis, *Nat. Commun.*, **7,** 10667 (2016).
21. A. Halder, M. Kilianova, B. Yang, E. C. Tyo, S. Seifert, R. Prucek, A. Panacek, P. Suchomel, O. Tomanec, D. J. Gosztola, D. Milde, H. H. Wang, L. Kvitek, R. Zboril, S. Vajda, Highly efficient Cu-decorated iron oxide nanocatalyst for low pressure CO_2 conversion, *Appl. Catal. B-Environ.*, **225,** 128 (2018).
22. E. D. Smit, M. M. Schooneveld, F. Cinquini, H. Bluhm, P. Sautet, F. M. De Groot, B. M. Weckhuysen, On the surface chemistry of iron oxides in reactive gas atmospheres, *Angew. Chem. Int. Ed*., **50,** 1584 (2011).
23. G. X. Chen, Y. Zhao, G. Fu, P. N. Duchesne, L. Gu, Y. P. Zheng, X. F. Weng, M. S. Chen, P. Zhang, C. W. Pao, J. F. Lee, N. F. Zheng, Interfacial effects in iron-nickel hydroxide-platinum nanoparticles enhance catalytic oxidation, *Science*, **344,** 495 (2014).
24. L. He, F. Weniger, H. Neumann, M. Beller, Synthesis, characterization, and application of metal nanoparticles supported on nitrogen-doped carbon: catalysis beyond electrochemistry, *Angew. Chem. Int. Ed*., **559,** 12582 (2016).
25. X. Lin, Z. Z. Nie, L. Y. Zhang, S. C. Mei, Y. Chen, B. S. Zhang, R. L. Zhu and Z. G. Liu, Nitrogen-doped carbon nanotubes encapsulate cobalt nanoparticles as efficient catalysts for aerobic and solvent-free selective oxidation of hydrocarbons, *Green Chem*., **19,** 2164 (2017).
26. W. Liu, L. L. Zhang, X. Liu, X. Y. Liu, X. F. Yang, S. Miao, W. T. Wang, A. Q. Wang, and T. Zhang, Discriminating catalytically active FeN_x species of atomically dispersed Fe-N-C catalyst for selective oxidation of the C-H bond, *J. Am. Chem. Soc*., **139,** 10790 (2017).
27. U. I. Kramm, I. Herrmann-Geppert, J. Behrends, K. Lips, S. Fiechter, and P. Bogdanoff, On an easy way to prepare metal-nitrogen doped carbon with exclusive presence of MeN_4-type sites active for the ORR, *J. Am. Chem. Soc*., **138,** 635 (2016).
28. T. H. Moss, and A. B. Robinson, Moessbauer experiments on iron(II) phthalocyanine, *Inorg. Chem*., **7,** 1692 (1968).
29. J. K. Li, S. Ghoshal, W. T. Liang, M. Sougrati, F. Jaouen, B. Halevi, S. McKinney, G. McCool, C. R. Ma, X. Yuan, Z. F. Ma, S. Mukerjee and Q. Y. Jia, Structural and mechanistic basis for the high activity of Fe-N-C catalysts toward oxygen reduction, *Energy Environ. Sci*., **9,** 2418 (2016).
30. N. R. Sahraie, U. I. Kramm, J. Steinberg1, Y. J. Zhang, A. Thomas, T. Reier, J. P. Paraknowitsch & P. Strasser, Quantifying the density and utilization of active sites in non-precious metal oxygen electroreduction catalysts, *Nat. Commun*., **6,** 8618 (2015).
31. A. Zitolo, V. Goellner, V. Armel, M. T. Sougrati, T. Mineva, L. Stievano, E. Fonda and F. Jaouen, Identification of catalytic sites for oxygen reduction in iron- and nitrogen-doped graphene materials, *Nat. Mater*., **14,** 937 (2015).
32. Q. Y. Jia, N. Ramaswamy, H. Hafiz, U. Tylus, K. Strickland, G. Wu, B. Barbiellini, A. Bansil, E. F. Holby, P. Zelenay, S. Mukerjee, Experimental observationof redox-induced Fe-N switching behavior as a determinant role for oxygen reduction activity, *ACS. Nano*., **9,** 12496 (2015).